# Generalist Bimanual Manipulation via Foundation Video Diffusion Models

Yao Feng<sup>1†</sup>, Hengkai Tan<sup>1\*</sup>, Xinyi Mao<sup>1</sup>, Guodong Liu<sup>1</sup>, Shuhe Huang<sup>1</sup>, Chendong Xiang<sup>1</sup>, Hang Su<sup>1</sup>, Jun Zhu<sup>1</sup>

<sup>1</sup>Dept. of Comp. Sci. and Tech., Institute for AI, BNRist Center, THBI Lab, Tsinghua-Bosch Joint ML Center, Tsinghua University y-feng23@mails.tsinghua.edu.cn

### **Abstract**

Bimanual robotic manipulation, which involves the coordinated control of two robotic arms, is foundational for solving challenging tasks. Despite recent progress in general-purpose manipulation, data scarcity and embodiment heterogeneity remain serious obstacles to further scaling up in bimanual settings. In this paper, we introduce VIdeo Diffusion for Action Reasoning (VIDAR), a two-stage framework that leverages large-scale, diffusion-based video pre-training and a novel masked inverse dynamics model for action prediction. We pre-train the video diffusion model on 750K multi-view videos from three real-world bimanual robot platforms, utilizing a unified observation space that encodes robot, camera, task, and scene contexts. Our masked inverse dynamics model learns masks to extract action-relevant information from generated trajectories without requiring pixel-level labels, and the masks can effectively generalize to unseen backgrounds. Our experiments demonstrate that with only 20 minutes of human demonstrations on an unseen robot platform (only 1% of typical data requirements), VIDAR generalizes to unseen tasks and backgrounds with strong semantic understanding, surpassing state-of-the-art methods. Our findings highlight the potential of video foundation models, coupled with masked action prediction, to enable scalable and generalizable robotic manipulation in diverse real-world settings.

# 1 Introduction

Bimanual manipulation—the coordinated control of two robotic arms—is central to many high-precision tasks in both industrial automation and domestic robotics. In contrast to single-arm manipulation, dual-arm skills enable stable object handling, in-hand reorientation, and multi-point contact control, which are essential for tasks such as cloth folding, liquid pouring, or tool-assisted assembly. Recent work on vision-language-action (VLA) foundation models [1, 2, 3, 4] has demonstrated promising results by leveraging large-scale multimodal pre-training, but extending these models to general-purpose bimanual settings remains highly nontrivial.

The challenge lies in the inherent complexity of bimanual control: the action space scales combinatorially with the number of controllable joints, while task success demands tight temporal coordination between arms, precise contact dynamics, and long-horizon planning. These properties substantially increase the data requirements and sensitivity to platform-specific variations. In practice, progress is limited by two fundamental bottlenecks. **First, data scarcity**: collecting large-scale, high-quality bimanual demonstrations is labor-intensive, expensive, and hardware-specific, resulting in orders-of-magnitude less data than what is available for single-arm or vision-language domains. **Second, embodiment heterogeneity**: differences in robot morphology, control frequency, and kinematics

<sup>\*</sup>Equal contribution; †: project lead

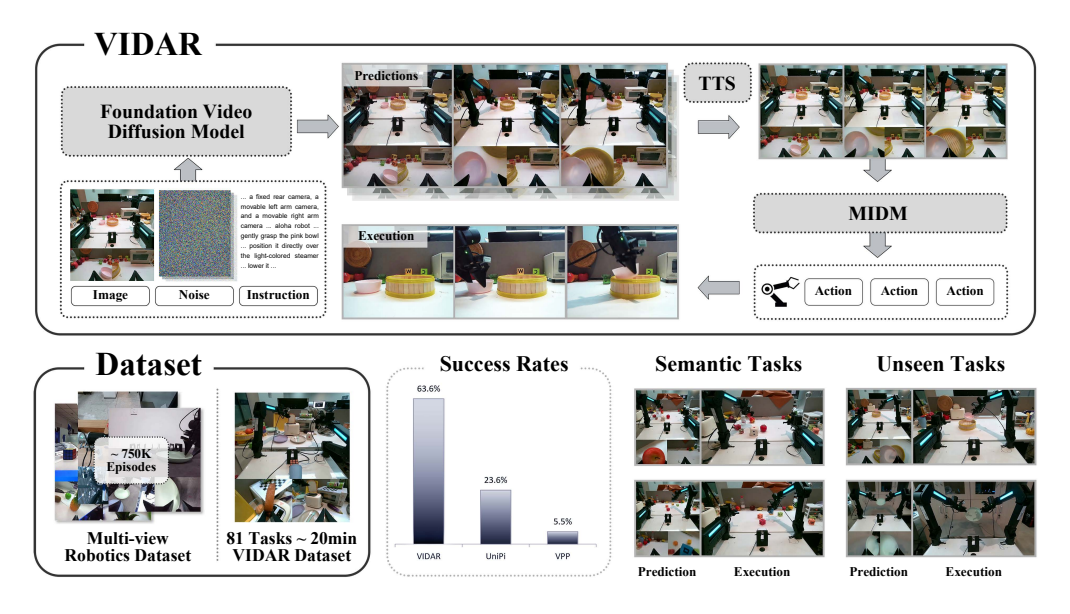


Figure 1: Overview of **VIdeo Diffusion for Action Reasoning (VIDAR)**, a foundation video diffusion model for video prediction and masked inverse dynamics model (MIDM) for action regression. Trained on 750K multi-view bimanual videos with test-time scaling (TTS) applied during testing, VIDAR can adapt to new robot platforms with 20 minutes of demonstrations with state-of-the-art performance and generalize to unseen tasks with strong semantic understanding.

lead to poor cross-platform transferability, requiring extensive robot-specific fine-tuning to adapt pre-trained models [5, 6].

To address these limitations, we propose **VIdeo Diffusion for Action Reasoning (VIDAR)**, as is shown in Figure 1. We train a foundation video diffusion model with 750K multi-view bimanual videos collected from three real-world robot platforms, where embodiment heterogeneity is handled by a unified observation space. Our key insight is that *pre-trained video prediction models can serve as transferable priors for robotic control*, provided they are adapted to the dynamics of physical interaction and grounded in action-relevant content. We further adopt test-time scaling [7] to enhance the performance of the foundation model when domain-specific data is scarce.

With limited human demonstrations, it is also non-trivial to translate domain-specific videos into corresponding actions. To solve this problem, we introduce a **Masked Inverse Dynamics Model** (**MIDM**) that learns to focus on and extract action-relevant regions in the generated frames, without requiring any pixel-level supervision. At test time, the learned masks generalize well in discarding action-irrelevant features, further enhancing stability and generalization.

Empirically, VIDAR achieves strong performance with only **20 minutes of human demonstrations** (3 demonstrations per task on average) in a previously unseen robotic platform, whereas prior methods [8, 3] require about 100 times more data. Moreover, VIDAR outperforms state-of-the-art baselines VPP [9] and UniPi [10] by 58% and 40% respectively. Also, it can generalize to novel tasks and backgrounds, with good semantic understanding.

#### Our main contributions are:

- We present the first large-scale video foundation model for bimanual manipulation, trained on 750K diverse demonstrations across three robot platforms with a unified observation space.
- We introduce a masked inverse dynamics model that learns to extract generalizable action-relevant features from generated videos without requiring segmentation labels.
- We demonstrate effective few-shot generalization with only 20 minutes of target-domain demonstrations, achieving state-of-the-art performance across unseen tasks and backgrounds.

Our results suggest that combining video generation and masked control prediction offers a scalable path toward general-purpose robotic manipulation in the wild.

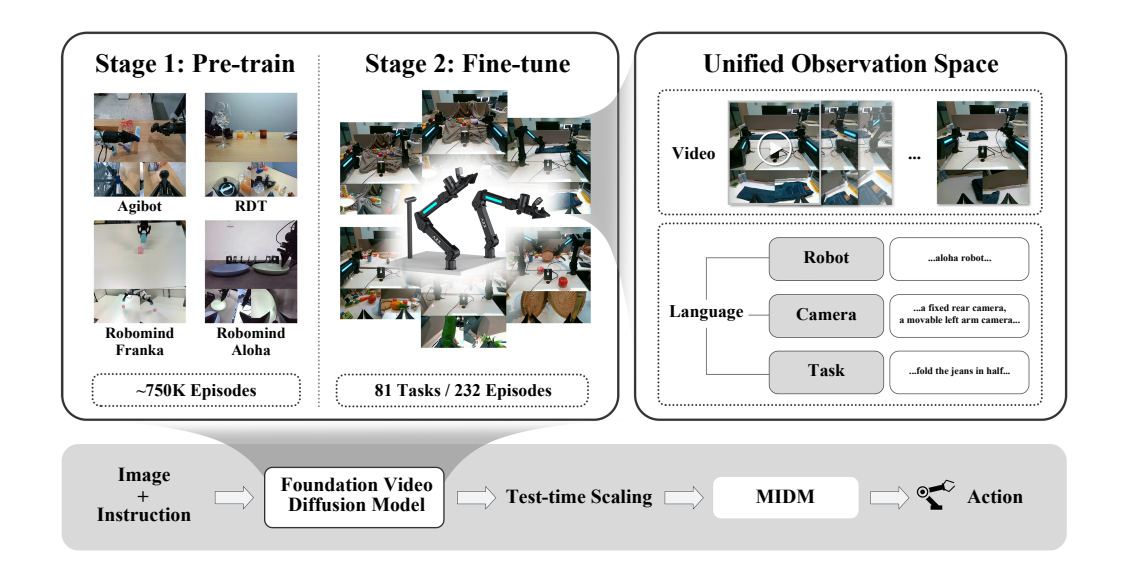


Figure 2: We introduce a unified observation space that integrates multi-view robotic videos and language instructions. This enables the training of a foundation video diffusion model on 750K multi-view bimanual robotic episodes, allowing it to generalize to unseen robot platforms with only 20 minutes of human demonstrations. At inference time, it generates multiple candidate videos, then applies test-time scaling (TTS) to select the most suitable one. We also propose the masked inverse dynamics model (MIDM), which learns masks to identify and attend to action-relevant regions for robust frame-based action regression.

#### 2 Method

In this section, we formally define our problem and describe the proposed VIDAR approach in detail. The overview of our method is shown in Figure 2.

#### 2.1 Problem Formulation

Let  $\mathcal L$  denote the language instruction space,  $\mathcal O$  the observation space, and  $\mathcal A$  the action space. Our objective is to learn a conditional robot manipulation policy  $\pi:\mathcal L\times\mathcal O\to\mathbb P(\mathcal A)$ , where  $\mathbb P(\cdot)$  represents the set of all probability measures over the given space. Directly learning this policy poses significant challenges, mainly due to the large volume of demonstrations required to achieve generation and generalization over three different modalities: language, observation, and action. For example, RDT-1B [3] collects 27 hours of human demonstrations for adaptation to the Aloha robot, which greatly limits its applicability to new platforms.

Our key insight is to introduce a unified intermediate domain in which the gaps between robot platforms are reduced, while still preserving all the information necessary for action prediction. In this way, we form a two-stage method, consisting of intermediate state prediction and action prediction. In the first stage, pre-training over existing embodied datasets can be applied with greater transferability; in the second stage, action prediction is also easier since the input only contains one modality. Here we choose the video space  $\mathcal V$  as the intermediate domain. In this way, we can decompose the policy:  $\pi = G \circ I$ , where  $G: \mathcal L \times \mathcal O \to \mathbb P(\mathcal V)$  is a video generation model and  $I: \mathcal V \to \mathcal A$  is an inverse dynamics model.

**Unified Observation Space.** By leveraging the video modality as an intermediate representation, data from heterogeneous embodiments can be mapped to a unified space. Denoting the number of cameras as V, we can define a unified observation space  $\mathcal{U} \subseteq \mathcal{L} \times \mathcal{O}$ :

$$\mathcal{U} = \{ \langle \mathbf{o}, \mathbf{l} \rangle | \mathbf{o} = \operatorname{aggregate}(\mathbf{I}^{(1)}, \mathbf{I}^{(2)}, \cdots, \mathbf{I}^{(V)}), \mathbf{l} = l_r + l_c + l_t, \},$$
(1)

where  $\operatorname{aggregate}(\mathbf{I}^{(1)}, \mathbf{I}^{(2)}, \cdots, \mathbf{I}^{(V)})$  are the aggregation of multi-view images (e.g., concatenation after proper down-sampling), and  $l_r$ ,  $l_c$ , and  $l_t$  are instructions related to the robotic platform, camera, and task, respectively. In this way, robot, camera, task, and multi-view information, instead of only task and single-view information, are provided as the condition for the video generation model, reducing the gap between pre-training and adaptation and enabling compositional generalization.

We choose the Aloha platform with three views as our bimanual robot in the target domain, since it is widely used and suitable for teleoperations [11, 3]. For our target robot, actions are defined as target joint/gripper positions without conditioning on the history, which means the inverse dynamics model can be viewed as sequential applications of a simpler mapping from one image to one action. With a little abuse of notation, we denote the simpler mapping as the inverse dynamics model throughout.

One important assumption underlying this approach is that the intermediate video modality contains all the information for action prediction. However, this assumption fails to hold for many robotic systems due to the specific platform setting, including the Aloha platform. In the pre-training part of Figure 2, we can see that the arm joints frequently fall outside the camera's field of view, even with three different views available. In our target domain, we adjust the center camera to a new position where two arms can be fully captured, shown in the fine-tuning part of Figure 2. In this way, our robotic platform differs from any platform we encountered during pre-training, serving as an ideal testbed for showing adaptation capability with scarce data.

#### 2.2 Video Generation Model

We adopt rectified flow [12, 13] models, which generate high-quality videos by modeling pixel flow over time. Specifically, the model parameterizes a flow function  $v: \mathcal{V} \times \mathbb{R} \times \mathcal{L} \to \mathcal{V}$ , which models the velocity of pixels as they transition from noisy video frames to target frames under certain conditions and time, leading to the following ODE over a video  $x_t$  (with  $x_0$  sampled from a Gaussian and  $x_1$  as the output video):

$$\frac{\mathrm{d}x_t}{\mathrm{d}t} = v(x_t, t, c), \quad t \in [0, 1]. \tag{2}$$

During training, we train the "velocity" v to approximate the constant flow from  $x_0$  to  $x_1$ . The flow matching loss is:

$$L_G = \mathbb{E}_{c,t,x_0,x_1} \left[ \| (x_1 - x_0) - v(tx_1 + (1-t)x_0, t, c) \|^2 \right].$$
 (3)

We also augment the model with an additional "unconditional" task  $\emptyset$  and jointly train on randomly sampled video pairs to enable classifier-free guidance. During inference, we can use any condition c in our unified observation space, and update the flow v using classifier-free guidance:

$$v'(x_t, t, c) = v(x_t, t, c) + \omega(v(x_t, t, c) - v(x_t, t, \emptyset)), \tag{4}$$

where  $\omega$  is a hyperparameter controlling the guidance strength. This new flow v' is used to generate videos by solving the ODE described in Eq. 2.

Embodied Pre-training and Fine-tuning on Unified Observation Space. To address the diversity and heterogeneity of real-world bimanual robots, we pre-train our video generation model on a large-scale corpus of approximately 750K open-sourced episodes, all projected into a unified observation space. This dataset includes episodes with three fixed camera views, a configuration common in bimanual setups [14, 15]. The primary challenge lies in harmonizing heterogeneous embodiments: different robots vary in camera placements, viewing angles, and sensor resolutions, leading to covariate shifts in perception. Moreover, wrist-mounted views often introduce task-irrelevant information, increasing input noise and model variance.

Unified Observation Construction. To mitigate this, we standardize each frame at timestep t by resizing less informative views (e.g., wrist-mounted) to smaller dimensions, and concatenating them with primary views along the channel dimension. Formally, each observation  $\mathbf{o}_t$  is constructed as  $\mathbf{o}_t = \bigoplus_{k=1}^V \gamma_k \cdot \phi_{r_k}(\mathbf{I}_t^{(k)})$ , where  $\mathbf{I}_t^{(k)}$  is the RGB image from camera k,  $\phi_{r_k}$  is a spatial resizing function,  $\gamma_k \in [0,1]$  is a confidence weight for view k. This operation produces a consistent tensor shape across platforms and preserves both semantic and kinematic context. We also incorporate dataset-specific metadata indicating the robot and camera view type to support domain adaptation.

During pre-training, episodes are uniformly sampled and used to train a conditional video diffusion model to generate temporally coherent rollouts conditioned on initial observations. At fine-tuning time, we apply the same preprocessing pipeline and perform supervised fine-tuning (SFT) on all model parameters using a small number of human demonstration episodes collected from the target platform.

**Test-time Scaling.** Diffusion-based video generation is inherently stochastic, leading to significant variance in the quality and task-relevance of sampled rollouts.

Naïvely sampling a single trajectory may result in incoherent or suboptimal generations, especially in cluttered or ambiguous scenes. To address this, we apply a test-time scaling strategy: given an observation prefix  $\mathbf{o}_1$ , we generate K candidate video trajectories  $\{\tilde{\mathbf{v}}_{1:T}^{(i)}\}_{i=1}^K$  using different random seeds. We then rank these trajectories using a pretrained evaluator (e.g., CLIP or a vision-language model)  $q_\eta$  and select the highest-scoring one, i.e.,  $\arg\max_i \ q_\eta(\tilde{\mathbf{v}}_{1:T}^{(i)})$ . This approach reduces sampling variance and consistently improves the quality of generated demonstrations with marginal computational overhead.

#### 2.3 Masked Inverse Dynamics Model

Inverse dynamics models often suffer from poor generalization due to the presence of background noise, texture biases, and visual distractions in high-dimensional observations. Explicitly localizing action-relevant regions is difficult without dense annotations. We introduce a masked inverse dynamics model (MIDM) that learns to focus on task-relevant regions via implicit mask prediction. The model consists of two components: (1) a mask prediction network U that outputs a spatial mask  $m \in [0,1]^{H \times W}$  from an input frame x, and (2) an action regression network R that predicts the action from the masked frame. Formally:

$$m = U(x), \quad \hat{a} = R(\text{round}(m) \odot x),$$

where  $\odot$  denotes element-wise multiplication. The model is trained with the following loss:

$$L_I = \mathbb{E}_{x,a} \left[ l(\hat{a} - a) + \lambda ||m||_1 \right],$$

where  $l(\cdot)$  may be any suitable loss (e.g., MSE), and we train it using straight-through estimators. Here, the second term promotes spatial sparsity, encouraging the model to focus on minimal, task-critical regions without any segmentation supervision. This enables robust generalization to unseen environments and backgrounds, as shown in our experiments (Section 3).

#### 3 Experiments

We want to prove the following hypotheses:

- H1: VIDAR achieves superior success rates with only 20 minutes of target domain demonstrations;
- **H2:** VIDAR generalizes effectively to unseen tasks and backgrounds;
- **H3:** Pre-training with a unified observation space benefits robot manipulation;
- **H4:** Masked inverse dynamics models exhibit greater generalization ability than the baseline.

#### 3.1 Experimental Setup

#### 3.1.1 Datasets

For pre-training, we utilize episodes sourced from Agibot-World [15], RoboMind [5], and RDT [3]. For Agibot-World, episodes are segmented into shorter clips using their frame-level annotations. As is required by the unified observation space, we provide descriptions of the robot type and camera placements in addition to the provided task instructions. The resulting pre-training dataset comprises 746,533 episodes.

For the target robot domain, we collect 20 minutes of human demonstration videos, covering 81 tasks across 232 episodes. This dataset is used to both fine-tune the video diffusion model and to train the masked inverse dynamics model. For more details of our datasets, see Appendix A.

#### 3.1.2 Training and Inference

We utilize Vidu 2.0 [16] as our video generation model. We train for 23,000 iterations with a batch size of 128, where the first 10,000 steps involve pre-training on the diverse robotics dataset, followed by 13,000 fine-tuning steps. To reduce inference costs, we uniformly downsample the training videos to 8 frames per second (fps). For the masked inverse dynamics model, we adopt the U-Net [17] structure as the mask prediction network and the ResNet [18] structure as the action regression network, with  $\lambda = 3 \times 10^{-3}$  (effects of  $\lambda$  are shown in Appendix C). We train it exclusively on the fine-tuning dataset. We use AdamW [19] for all our training.

We use open-loop control for VIDAR; the videos are generated in a single batch, without subsequent generation after the initial run. Using 8 NVIDIA Ampere-series 80GB GPUs, generating one video with 60 frames (7.5 seconds duration at 8fps) costs about 25 seconds. For test-time scaling, we choose K=3, and three videos with different random seeds are generated in parallel, evaluated by GPT-40 [20]. More details of training and inference can be found in Appendix B.

We acknowledge that Vidu 2.0 is not open source. To demonstrate the generality of our approach, we also perform small-scale experiments using the open-source HunyuanVideo model [21]. Related results are shown in Appendix E.

#### 3.1.3 Baselines

We perform preliminary experiments over multiple baselines and find that adaptation with only 20 minutes of videos and about 3 demonstrations per task is too challenging for vision-language-action models. Thus, we choose two baselines that also incorporate video-level prior knowledge: UniPi and VPP. To ensure fair comparison, we reproduce these methods over the advanced Vidu 2.0 model.

**UniPi.** We fine-tune the Vidu 2.0 model directly on our demonstration data, without any additional pre-training on our large robotics dataset. Additionally, we train an inverse dynamics model using a ResNet architecture.

**VPP.** We use the same checkpoint for the video generation model as our method, and train a diffusion model to generate short action sequences based on the latent features during one-step video generation and CLIP [22] embeddings of the task instructions. Notably, they use closed-loop control, which means new action sequences are generated and executed after previous executions.

#### 3.2 Experimental Results

**H1: Success Rates.** We test two baseline methods and our method over 16 tasks under three scenarios: seen task and background (six tasks), unseen task (four tasks), and unseen background (six tasks). Detailed explanations are as follows:

- Seen Tasks & Backgrounds: three pick-and-place tasks (e.g., grasp tomato using left arm), two daily-life tasks (e.g., flip dice using right arm), and one bimanual task (lift the basket). The background we use is a cluttered office desk setup, featuring several computers situated behind the workspace.
- Unseen Tasks: three daily-life tasks (e.g., stack the bowl on the steamer using the left arm) and two semantic tasks (e.g., grasp the shortest bread using the left arm).
- Unseen Backgrounds: two pick-and-place tasks (e.g., grasp a tomato using the left arm) and four daily-life tasks (e.g., flip a dice using the left arm). For unseen backgrounds, we include a studio setup with a typical green screen and a daily workspace setting with two cupboards containing robot supplies, which exhibit reflective surfaces.

The success rates are shown in Table 1. We find that our method achieves superior success rates over all three scenarios, demonstrating the effectiveness of our method. More details can be found in Appendix C.

**H2: Generalization Ability.** Quantitative results of our superior generation ability are shown in unseen scenarios of Table 1. We also provide some demonstrations in Figure 3, where VIDAR demonstrates robust generalization to unseen tasks and backgrounds with strong semantic understanding. In Appendix D, we present more visualizations, including failure cases.

Table 1: Success rates of different methods and configurations over robot manipulation tasks. VIDAR achieves high success rates across all three scenarios, with great generalization ability to unseen tasks and backgrounds.

Methods	Seen Tasks & Backgrounds	Unseen Tasks	Unseen Backgrounds
VPP	4.5%	13.3%	0.0%
UniPi	36.4%	6.7%	22.2%
VIDAR (Ours)	<b>68.2</b> %	66.7%	55.6%



Figure 3: Videos of predictions (left) and corresponding executions (right) of VIDAR for challenging tasks. It can handle unseen tasks and unseen backgrounds with strong semantic understanding.

Table 2: VBench video quality measurements for different video model configurations in the unseen target domain. Embodied pre-training over the unified observation space benefits video generation.

Configurations	Subject Consistency	Background Consistency	Imaging Quality
Vidu 2.0	0.565	0.800	0.345
+ Embodied Pre-training	<b>0.855</b>	<b>0.909</b>	<b>0.667</b>

Table 3: Training and testing success rates and testing  $1_1$  errors of different inverse dynamics models. Both the baseline and MIDM achieve high performances during training, but MIDM generalizes better during test time.

Inverse Dynamics Models	Training Accuracy	Testing Accuracy	Testing $l_1$ Error
ResNet	99.9%	24.3%	0.0430
MIDM (Ours)	99.9%	<b>49.0</b> %	<b>0.0308</b>

**H3:** Effectiveness of Pre-training. We evaluate the video generation quality of the original Vidu 2.0 model and our pre-trained version over the unseen target domain using VBench [23]. As is shown in Table 2, we find that pre-training using large-scale robotic videos under our unified observation space enhances both the consistency and quality of generated frames, which are important for robot control tasks.

**H4:** Effectiveness of MIDM. Based on empirical observations of the Aloha robot's error tolerances, we define a successful prediction as having a maximum infinity norm error of less than 0.06 for joint positions and less than 0.6 for gripper positions, for both arms. Using this criterion, we evaluate the success rates of our masked inverse dynamics model (MIDM) and a ResNet baseline on both training and testing sets. The results, presented in Table 3, show that our MIDM demonstrates superior generalization compared to the baseline. Additionally, examples of the learned masks are provided in Figure 4. Without any additional supervision, MIDM effectively captures action-relevant features and generalizes well to unseen backgrounds.

## 3.3 Ablation Study

We conduct an ablation study of our method by evaluating success rates on the same tasks presented in Table 1. The results are summarized in Table 4, where "w/o MIDM" means using the ResNet

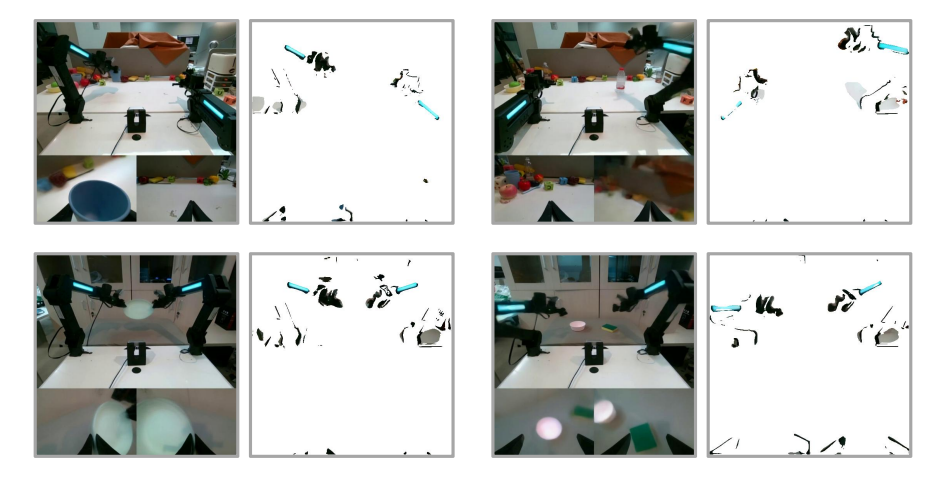


Figure 4: Input images and corresponding masked images learned by the masked inverse dynamic model (MIDM). The two cases at the top are from a seen background, while the other two are from an unseen background. The predicted masks focus on the essential parts of robotic arms and have great generalization ability.

Table 4: Ablation study of VIDAR, where "w/o MIDM" means using the ResNet baseline. In three scenarios, both masked inverse dynamics models and test-time scaling are beneficial to the success rates.

Configurations	Seen Tasks & Backgrounds	Unseen Tasks	Unseen Backgrounds
VIDAR w/o TTS	45.5%	33.3%	44.4%
VIDAR w/o MIDM	59.1%	26.7%	22.2%
VIDAR	68.2%	66.7%	55.6%

baseline. We find that both masked inverse dynamics models and test-time scaling are beneficial to the success rates.

#### 4 Related Work

Vision-Language-Action Models (VLAs). Vision-Language-Action (VLA) models integrate perception, language understanding, and action generation to enable general-purpose embodied intelligence. However, existing VLA systems rely heavily on large-scale, task-specific datasets—often requiring hundreds of thousands of trajectories—to achieve robust performance. For instance, RT-1 [8] uses 130K real-world episodes, while RT-2 [24] scales to 1B image-text pairs. Recent works like OpenVLA [2], Octo [25], Pi0 [26], and RDT-1B [3] further expand to millions of demonstrations across diverse embodiments. Despite these efforts, such data-intensive pipelines present a scalability bottleneck and limit generalization to novel tasks and domains, motivating more data-efficient and transferable alternatives.

**Video Generation Models for Embodied AI.** Video generation models for embodied AI predict future scene dynamics to assist robotic planning and policy learning. Current works such as UniPi [27], RoboDreamer [28], Gen2Act [29], and GR-1 [30] mainly adopt text-conditioned video generation with a fixed single-camera view, demonstrating how a single-arm robot physically compliantly executes a series of actions. Additionally, Genie 2 [31] generates interactive 3D environments via autoregressive latent diffusion, enabling scalable training for embodied agents. These models implicitly encode physical laws through video synthesis, reducing reliance on real-world robotics data. However, current works mostly remain limited to single-arm robots and rely on a single camera view, which restricts their applicability in more complex real-world scenarios.

Coupled Video Generation and Action Synthesis. Recent efforts couple video generation with action synthesis to enhance physical consistency and interoperability. For instance, Video-Prediction-Policy (VPP) [9] learns implicit inverse dynamics conditioned on future representations predicted by video diffusion model, while UVA [32] unifies video-action latent spaces with lightweight diffusion heads. Other works, such as VidMan [33] and Dreamitate [34], integrate low-level action representations with video prediction to predict actions. These approaches bridge spatiotemporal dynamics between vision and action, offering novel solutions for complex manipulation tasks. However, these approaches require end-to-end joint training of video generation and action prediction models, which limits their flexibility and adaptability. Integrating a more advanced video generation model would necessitate retraining the entire system.

## 5 Conclusion and Broader Impact

We presented VIDAR, a generalizable framework for bimanual robotic manipulation that addresses the core challenges of data scarcity and embodiment heterogeneity. By combining large-scale, diffusion-based video pretraining over a unified observation space with a masked inverse dynamics model, VIDAR enables accurate action prediction from multi-view visual observations and language instructions, requiring only minimal demonstrations in new environments. Our experiments demonstrate that VIDAR consistently outperforms existing methods and exhibits strong generalization to unseen tasks and backgrounds, highlighting its capacity for semantic understanding and transfer.

#### References

- [1] Abby O'Neill et al. "Open X-Embodiment: Robotic Learning Datasets and RT-X Models: Open X-Embodiment Collaboration". In: *IEEE International Conference on Robotics and Automation, ICRA 2024, Yokohama, Japan, May 13-17, 2024.* IEEE, 2024, pp. 6892–6903.
- [2] Moo Jin Kim et al. "OpenVLA: An Open-Source Vision-Language-Action Model". In: *Conference on Robot Learning, 6-9 November 2024, Munich, Germany*. Ed. by Pulkit Agrawal, Oliver Kroemer, and Wolfram Burgard. Vol. 270. Proceedings of Machine Learning Research. PMLR, 2024, pp. 2679–2713.
- [3] Songming Liu et al. "RDT-1B: a Diffusion Foundation Model for Bimanual Manipulation". In: *CoRR* abs/2410.07864 (2024).
- [4] Yunhao Zhang and Junchi Yan. "Crossformer: Transformer Utilizing Cross-Dimension Dependency for Multivariate Time Series Forecasting". In: *The Eleventh International Conference on Learning Representations, ICLR 2023, Kigali, Rwanda, May 1-5, 2023*. OpenReview.net, 2023.
- [5] Kun Wu et al. "RoboMIND: Benchmark on Multi-embodiment Intelligence Normative Data for Robot Manipulation". In: *CoRR* abs/2412.13877 (2024).
- [6] Guanxing Lu et al. "AnyBimanual: Transferring Unimanual Policy for General Bimanual Manipulation". In: *CoRR* abs/2412.06779 (2024).
- [7] Aaron Jaech et al. "OpenAI o1 System Card". In: *CoRR* abs/2412.16720 (2024).
- [8] Anthony Brohan et al. "RT-1: Robotics Transformer for Real-World Control at Scale". In: *Robotics: Science and Systems XIX, Daegu, Republic of Korea, July 10-14, 2023*. Ed. by Kostas E. Bekris et al. 2023.
- [9] Yucheng Hu et al. "Video Prediction Policy: A Generalist Robot Policy with Predictive Visual Representations". In: *CoRR* abs/2412.14803 (2024).
- [10] Yilun Du et al. "Learning Universal Policies via Text-Guided Video Generation". In: Advances in Neural Information Processing Systems 36: Annual Conference on Neural Information Processing Systems 2023, NeurIPS 2023, New Orleans, LA, USA, December 10 16, 2023. Ed. by Alice Oh et al. 2023.
- [11] Tony Z. Zhao et al. "Learning Fine-Grained Bimanual Manipulation with Low-Cost Hardware". In: Robotics: Science and Systems XIX, Daegu, Republic of Korea, July 10-14, 2023. Ed. by Kostas E. Bekris et al. 2023.
- [12] Yaron Lipman et al. "Flow Matching for Generative Modeling". In: *The Eleventh International Conference on Learning Representations, ICLR 2023, Kigali, Rwanda, May 1-5, 2023*. OpenReview.net, 2023.
- [13] Xingchao Liu, Chengyue Gong, and Qiang Liu. "Flow Straight and Fast: Learning to Generate and Transfer Data with Rectified Flow". In: *The Eleventh International Conference on Learning Representations, ICLR 2023, Kigali, Rwanda, May 1-5, 2023.* OpenReview.net, 2023.
- [14] Zipeng Fu, Tony Z. Zhao, and Chelsea Finn. "Mobile ALOHA: Learning Bimanual Mobile Manipulation with Low-Cost Whole-Body Teleoperation". In: CoRR abs/2401.02117 (2024).
- [15] AgiBot-World-Contributors et al. "AgiBot World Colosseo: A Large-scale Manipulation Platform for Scalable and Intelligent Embodied Systems". In: *CoRR* abs/2503.06669 (2025).
- [16] Fan Bao et al. "Vidu: a Highly Consistent, Dynamic and Skilled Text-to-Video Generator with Diffusion Models". In: *CoRR* abs/2405.04233 (2024).
- [17] Olaf Ronneberger, Philipp Fischer, and Thomas Brox. "U-Net: Convolutional Networks for Biomedical Image Segmentation". In: Medical Image Computing and Computer-Assisted Intervention - MICCAI 2015 - 18th International Conference Munich, Germany, October 5 - 9, 2015, Proceedings, Part III. Ed. by Nassir Navab et al. Vol. 9351. Lecture Notes in Computer Science. Springer, 2015, pp. 234–241.
- [18] Huazhi Xu, Xiaoyan Luo, and Wencong Xiao. "Multi-residual unit fusion and Wasserstein distance-based deep transfer learning for mill load recognition". In: *Signal Image Video Process.* 18.4 (2024), pp. 3187–3196.
- [19] Ilya Loshchilov and Frank Hutter. "Decoupled Weight Decay Regularization". In: 7th International Conference on Learning Representations, ICLR 2019, New Orleans, LA, USA, May 6-9, 2019. OpenReview.net, 2019.
- [20] Aaron Hurst et al. "GPT-40 System Card". In: CoRR abs/2410.21276 (2024).

- [21] Weijie Kong et al. "HunyuanVideo: A Systematic Framework For Large Video Generative Models". In: CoRR abs/2412.03603 (2024).
- [22] Alec Radford et al. "Learning Transferable Visual Models From Natural Language Supervision". In: *Proceedings of the 38th International Conference on Machine Learning, ICML 2021, 18-24 July 2021, Virtual Event.* Ed. by Marina Meila and Tong Zhang. Vol. 139. Proceedings of Machine Learning Research. PMLR, 2021, pp. 8748–8763.
- [23] Ziqi Huang et al. "VBench: Comprehensive Benchmark Suite for Video Generative Models". In: IEEE/CVF Conference on Computer Vision and Pattern Recognition, CVPR 2024, Seattle, WA, USA, June 16-22, 2024. IEEE, 2024, pp. 21807–21818.
- [24] Brianna Zitkovich et al. "RT-2: Vision-Language-Action Models Transfer Web Knowledge to Robotic Control". In: *Conference on Robot Learning, CoRL 2023, 6-9 November 2023, Atlanta, GA, USA*. Ed. by Jie Tan, Marc Toussaint, and Kourosh Darvish. Vol. 229. Proceedings of Machine Learning Research. PMLR, 2023, pp. 2165–2183.
- [25] Dibya Ghosh et al. "Octo: An Open-Source Generalist Robot Policy". In: *Robotics: Science and Systems XX, Delft, The Netherlands, July 15-19, 2024.* Ed. by Dana Kulic et al. 2024.
- [26] Kevin Black et al. " $\pi_0$ : A Vision-Language-Action Flow Model for General Robot Control". In: *CoRR* abs/2410.24164 (2024).
- [27] Yilun Du et al. "Learning Universal Policies via Text-Guided Video Generation". In: Advances in Neural Information Processing Systems 36: Annual Conference on Neural Information Processing Systems 2023, NeurIPS 2023, New Orleans, LA, USA, December 10 16, 2023. Ed. by Alice Oh et al. 2023.
- [28] Siyuan Zhou et al. "RoboDreamer: Learning Compositional World Models for Robot Imagination". In: Forty-first International Conference on Machine Learning, ICML 2024, Vienna, Austria, July 21-27, 2024. OpenReview.net, 2024.
- [29] Homanga Bharadhwaj et al. "Gen2Act: Human Video Generation in Novel Scenarios enables Generalizable Robot Manipulation". In: *CoRR* abs/2409.16283 (2024).
- [30] Hongtao Wu et al. "Unleashing Large-Scale Video Generative Pre-training for Visual Robot Manipulation". In: *The Twelfth International Conference on Learning Representations, ICLR* 2024, Vienna, Austria, May 7-11, 2024. OpenReview.net, 2024.
- [31] Jack Parker-Holder et al. "Genie 2: A Large-Scale Foundation World Model". In: (2024).
- [32] Shuang Li et al. "Unified Video Action Model". In: CoRR abs/2503.00200 (2025).
- [33] Youpeng Wen et al. "VidMan: Exploiting Implicit Dynamics from Video Diffusion Model for Effective Robot Manipulation". In: *Advances in Neural Information Processing Systems 38:*Annual Conference on Neural Information Processing Systems 2024, NeurIPS 2024, Vancouver, BC, Canada, December 10 15, 2024. Ed. by Amir Globersons et al. 2024.
- [34] Junbang Liang et al. "Dreamitate: Real-World Visuomotor Policy Learning via Video Generation". In: *Conference on Robot Learning, 6-9 November 2024, Munich, Germany*. Ed. by Pulkit Agrawal, Oliver Kroemer, and Wolfram Burgard. Vol. 270. Proceedings of Machine Learning Research. PMLR, 2024, pp. 3943–3960.

Table 5: Detailed information about datasets. Dataset instructions correspond to the robot and camera components of the unified observation space (see Figure 2).

Dataset	Size	Dataset Instructions
Agibot	726,843	The whole scene is in a realistic, industrial art style with three views: a fixed high camera, a movable left arm camera, and a movable right arm camera. The genie-1 robot is currently performing the following task:
RDT	6,023	The whole scene is in a realistic, industrial art style with three views: a fixed front camera, a movable left arm camera, and a movable right arm camera. The aloha robot is currently performing the following task:
RoboMind Franka	6,395	The whole scene is in a realistic, industrial art style with three views: a fixed camera on the opposite side, a fixed left camera, and a fixed right camera. The franka robot is currently performing the following task:
RoboMind Aloha	7,272	The whole scene is in a realistic, industrial art style with three views: a fixed front camera, a movable left arm camera, and a movable right arm camera. The aloha robot is currently performing the following task:
VIDAR	232	The whole scene is in a realistic, industrial art style with three views: a fixed rear camera, a movable left arm camera, and a movable right arm camera. The aloha robot is currently performing the following task:

#### A Dataset Details

The details of our datasets are presented in Table 5, with corresponding visualizations shown in Figure 5. We filter out episodes with fewer than three views or shorter than four seconds, and we further segment lengthy episodes in the Agibot dataset. For each dataset, we provide information about the associated robot and camera setups, which form part of the unified observation space. During pre-training, sampling ratios for each dataset are set proportionally to their sizes. It is worth noting that our VIDAR dataset differs from all pre-training datasets in these aspects, and we additionally leverage GPT-40 to augment its task annotations.

## **B** Training and Inference Details

Using 64 NVIDIA Ampere-series 80GB GPUs, we train Vidu 2.0 for 23,000 iterations (10,000 for pre-training and the remainder for fine-tuning), which takes about 64 hours. Note that for all fine-tuning procedures, we employ full-parameter fine-tuning. For MIDM, we use 8 NVIDIA Hopperseries 80GB GPUs for 60,000 training iterations, taking about 5 hours. Additional MIDM parameters are provided in Table 6.

During inference, the video diffusion models are deployed in the cloud, while only the lightweight MIDM is executed locally. For test-time scaling, we uniformly sample 5-7 frames from the generated videos and use GPT-40 to select the best result.

## C Additional Experimental Results

A more detailed version of Table 1 is provided in Table 7. We also investigate the impact of the parameter  $\lambda$  in MIDM, with results summarized in Table 8 and illustrated in Figure 6. Notably,  $\lambda = 3 \times 10^{-3}$  yields the best performance.

#### **D** Additional Visualizations of VIDAR

More demonstrations, including two failed cases, are shown in Figure 7.



Figure 5: Visualizations of datasets. The pre-training datasets feature a variety of robots and camera configurations, whereas our VIDAR dataset distinctively differs from all of these settings.

Table 6: Parameters of MIDM.

Tuble 6. Turumeters 61 Milbin.		
Values		
92 Million		
5		
ResNet-50		
Smoothed $l_1$ Loss		
$2 \times 10^{-5}$		
6000 Steps		
(0.9, 0.999)		
$10^{-8}$		
$10^{-2}$		

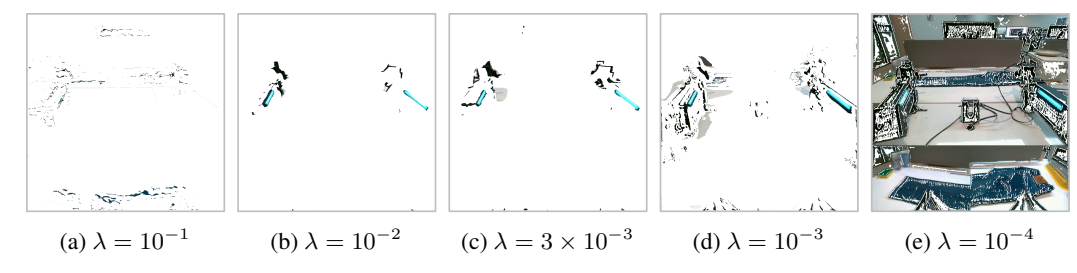


Figure 6: Masked images learned by the masked inverse dynamic model (MIDM) with different values of  $\lambda$ .

Table 7: Detailed success rates of various methods and configurations on robot manipulation tasks. "L," "R," and "B" indicate the use of the left arm, right arm, or both arms, respectively. "w/o TTS" and "w/o MIDM" correspond to the ablation settings described in Table 4.

Scenarios/Tasks Success Rates of Different Methods/Configuration				onfigurations	
Seen Tasks & Backgrounds	UniPi	VPP	VIDAR	w/o TTS	w/o MIDM
Grasp the Tomato (L)	60.0%	0.0%	60.0%	60.0%	80.0%
Grasp the Tomato (R)	20.0%	0.0%	80.0%	60.0%	60.0%
Lift the Basket (B)	66.7%	0.0%	66.7%	33.3%	33.3%
Flip the Dice to Point One on the Top (L)	0.0%	33.3%	33.3%	0.0%	33.3%
Grab the Bottle (L)	0.0%	0.0%	66.7%	33.3%	33.3%
Get the Toast from the Toaster (L)	66.7%	0.0%	100.0%	66.7%	100.0%
Total	36.4%	4.5%	68.2%	45.5%	59.1%
Unseen Tasks	UniPi	VPP	VIDAR	w/o TTS	w/o MIDM
Place the Bowl on the Steamer (L)	0.0%	0.0%	66.7%	66.7%	33.3%
Grasp the Shortest Bread (L)	0.0%	0.0%	66.7%	33.3%	0.0%
Grasp the Shortest Bread (R)	0.0%	0.0%	66.7%	33.3%	33.3%
Wipe the Table with Rag (L)	33.3%	33.3%	66.7%	33.3%	66.7%
Wipe the Table with Rag (R)	0.0%	33.3%	66.7%	0.0%	0.0%
Total	6.7%	13.3%	66.7%	33.3%	26.7%
Unseen Backgrounds	UniPi	VPP	VIDAR	w/o TTS	w/o MIDM
Grasp the Tomato (L)	0.0%	0.0%	66.7%	33.3%	0.0%
Flip the Die to Point One on the Top (L)	0.0%	0.0%	33.3%	33.3%	0.0%
Flip the Die to Point One on the Top (R)	0.0%	0.0%	33.3%	0.0%	0.0%
Pick the Carrot on the Green Plate (L)	33.3%	0.0%	33.3%	66.7%	0.0%
Place the Bowl on the Plate (L)	33.3%	0.0%	66.7%	66.7%	33.3%
Place the Bowl on the Plate (R)	66.7%	0.0%	100.0%	66.7%	100.0%
Total	22.2%	0.0%	55.6%	44.4%	22.2%

Table 8: Analysis of hyperparameter  $\lambda$  in the masked inverse dynamics model. The success rates are robust over a large range, and  $\lambda=3\times10^{-3}$  achieves the best performance.

λ	Training Accuracy	Testing Accuracy	Testing $l_1$ Error
$10^{-1}$	99.1%	7.1%	0.0670
$10^{-2}$	99.8%	39.9%	0.0331
$3 \times 10^{-3}$	99.9%	49.0%	0.0308
$10^{-3}$	99.9%	40.7%	0.0338
$10^{-4}$	99.8%	24.4%	0.0461



Figure 7: Videos of predictions (left) and corresponding executions (right) of VIDAR for more challenging tasks. Both successful and failed cases are presented.

Table 9: Parameters of the HunyuanVideo Model.

Parameters	Values
Number of Parameters	13 Billion
Learning Rate (Pre-train)	$1 \times 10^{-4}$
Learning Rate (Fine-tune)	$5 \times 10^{-5}$
Warm-up	500 Steps
Optimizer	AdamW
AdamW $\beta$	(0.9, 0.999)
AdamW $\epsilon$	$10^{-8}$
AdamW Weight Decay	0

Table 10: Success rates of VIDAR reproduced using the HunyuanVideo Model.

Tasks	Success Rates
Grasp the Apple (Seen Task)	75.0%
Grab the Bottle (Seen Task)	100.0%
Grasp the Cup by its Handle (Seen Task)	25.0%
Lift the Steamer (Unseen Task)	50.0%
Grasp the Apple and Put it into the Steamer (Unseen Task)	100.0%
Stack One Cube on Top of the Other Cube (Unseen Task)	20.0%
Total	58.3%

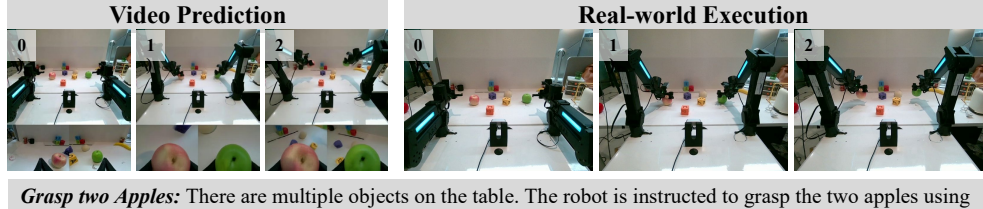
# E Reproduction using the HunyuanVideo Model

We also reproduced our results using the open-source HunyuanVideo Model. The training parameters are detailed in Table 9. Utilizing 64 NVIDIA Hopper-series 80GB GPUs, we trained the model for 12,000 iterations (10,000 for pre-training and the remainder for fine-tuning), which required approximately 54 hours.

Due to limited resources, we evaluated the model on six tasks. The results are presented in Table 10 and Figure 8. We plan to open-source our implementations related to both the HunyuanVideo Model and our MIDM.

## F Hardware Details

Hardware details are shown in Figure 9 and Table 11.



**Grasp two Apples:** There are multiple objects on the table. The robot is instructed to grasp the two apples using both arms. The robot needs to: **(0) identify the two apples among all objects**, **(1)** secure its hold on both apples, **(2)** lift the apples simultaneously as required.



Stack the cubes: There are multiple cubes on the table. The robot is instructed to stack the green cube on the blue cube using its right arm. The robot needs to: (0) identify the both cubes among all cubes, (1) grasp the green cube, (2) put it on top of the blue cube as required.



Lift the steamer: There is a steamer on the table. The robot is instructed to lift the steamer using both arms. The robot needs to: (0) align the grippers with the edge of the steamer, (1) secure its hold on the steamer, (2) lift upwards simultaneously.

Figure 8: Videos of predictions (left) and corresponding executions (right) of VIDAR reproduced using the HunyuanVideo model for challenging tasks.



Figure 9: Our robotic platform.

Table 11: Hardware Information.

Parameters	Values
Degree of Freedom	$2 \times (6+1) = 14$
Cameras	3 RGB Cameras
Arm weight	$3.9\mathrm{kg}$
Arm Valid Payload	$1.0\mathrm{kg}$
Arm Reach	$0.6\mathrm{m}$
Arm Repeatability	$1\mathrm{mm}$
Gripper Range	$0 - 80 \mathrm{mm}$
Gripper Max Force	$10\mathrm{N}$